Supporting information

Plasmon 3D Electron Tomography and Local Electric-field Enhancement of Engineered Plasmonic Nano-antennas

B. S. Archanjo[1,2], T. L. Vasconcelos[1], B. S. Oliveira[1], C. Song[2], F. Allen[2,3], C. A. Achete[1], P. Ercius[2]

1 Divisao de Metrologia de Materiais, Instituto Nacional de Metrologia, Qualidade e Tecnologia (INMETRO), Duque de Caxias, RJ 25250-020, Brazil

2 National Center for Electron Microscopy, Molecular Foundry, Lawrence Berkeley National Laboratory, 1 Cyclotron Rd., Berkeley, California 94720, United States

3 Department of Materials Science and Engineering, University of California, Berkeley, 210 Hearst Ave., Berkeley, California 94720, United States

Email: bsarchanjo@inmetro.gov.br

Number of pages: 8

Number of figures: 9

Number of Tables: 1

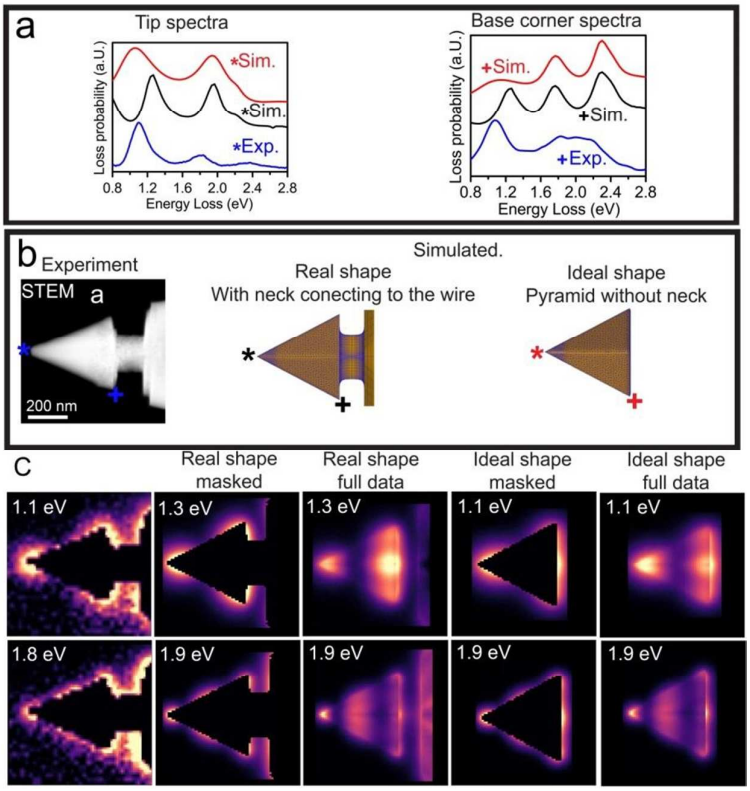

Fig. S1 – Supplementary to Fig. 1 of the main text. a) EELS spectra of the simulated ideal shape (floating pyramid without the notch) in red and real shape (with the notch). Experimental EELS curves are in black. Spectra in left are from the tip (around 10 nm far) of the nanopyramid and spectra in right is from one base corner of the nanopyramid as respectively shown in b. b) From left to right STEM image of the nanopyramid, simulated real shape (with notch) and ideal shape schemes. c) EELS maps of the two plasmonic modes observed in simulated and experimental EELS spectra in the tip. See also supplementary Video 1.

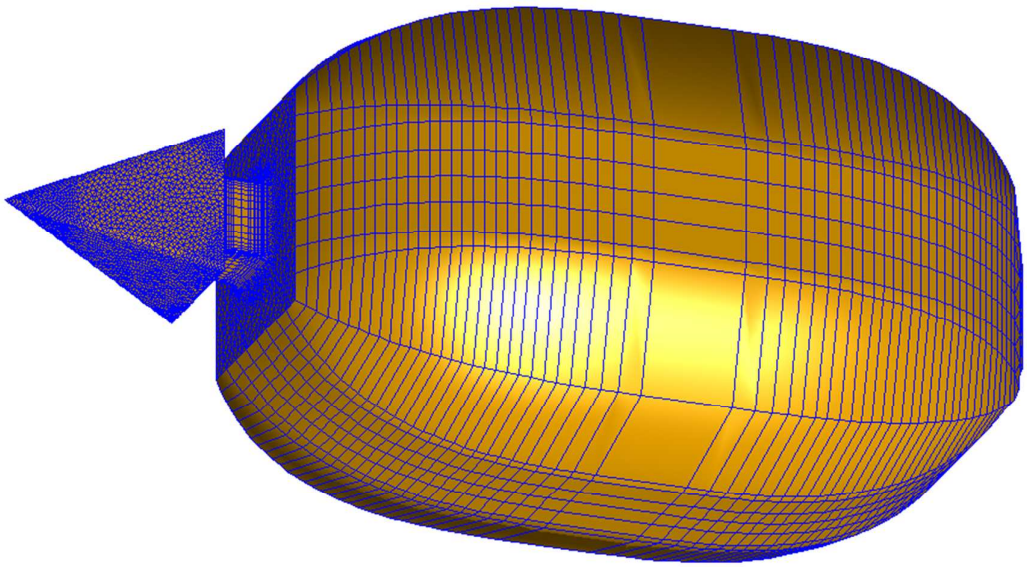

Fig. S2 – Supplementary to Fig. 1 of the main text. Full image showing the mesh of the nanopyramid real shape with the notch and the gold wire body. In the simulation the gold wire is about 5 times bigger than the nanopyramid, therefore generating plasmons only in far infrared which do not interfere with the LSPR modes of the nanopyramid.

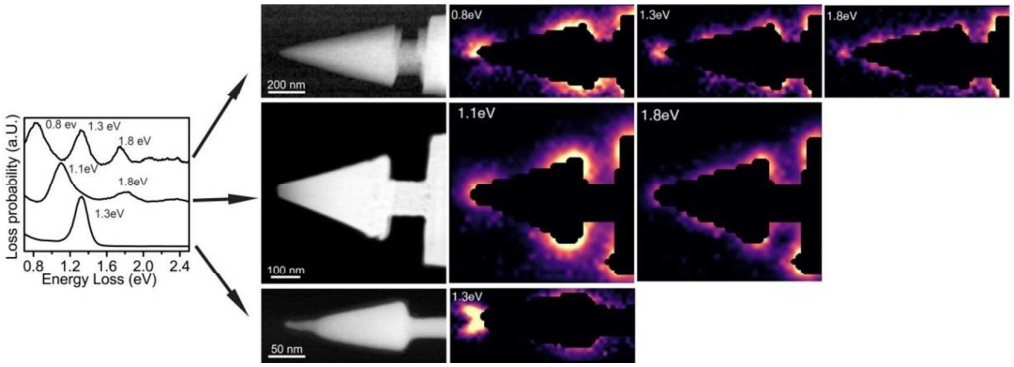

Fig. S3 –EELS spectra, STEM images and 2D EELS maps for the LSRP modes of the experimental data from the three nanopyramids used in Fig. 2 in the main text. From top to bottom we respectively show the results of nanopyramids having 750 nm (θ=30°), 450 nm (θ=45°) and 160 nm (θ=18°) for lateral length *L* (opening angle θ). See also Video 2 for animated maps.

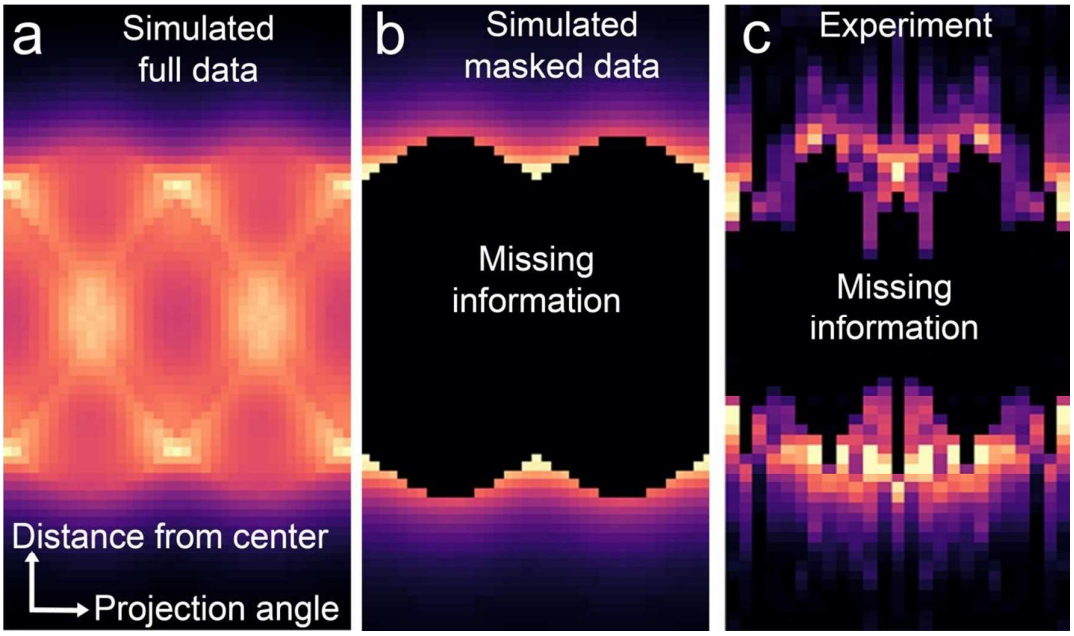

Fig. S4 – Simulated (having full information and masked) and experimental sinograms, from a slice in the middle of the nanopyramid, showing the missing information in the EELS maps when the beam crosses the sample.

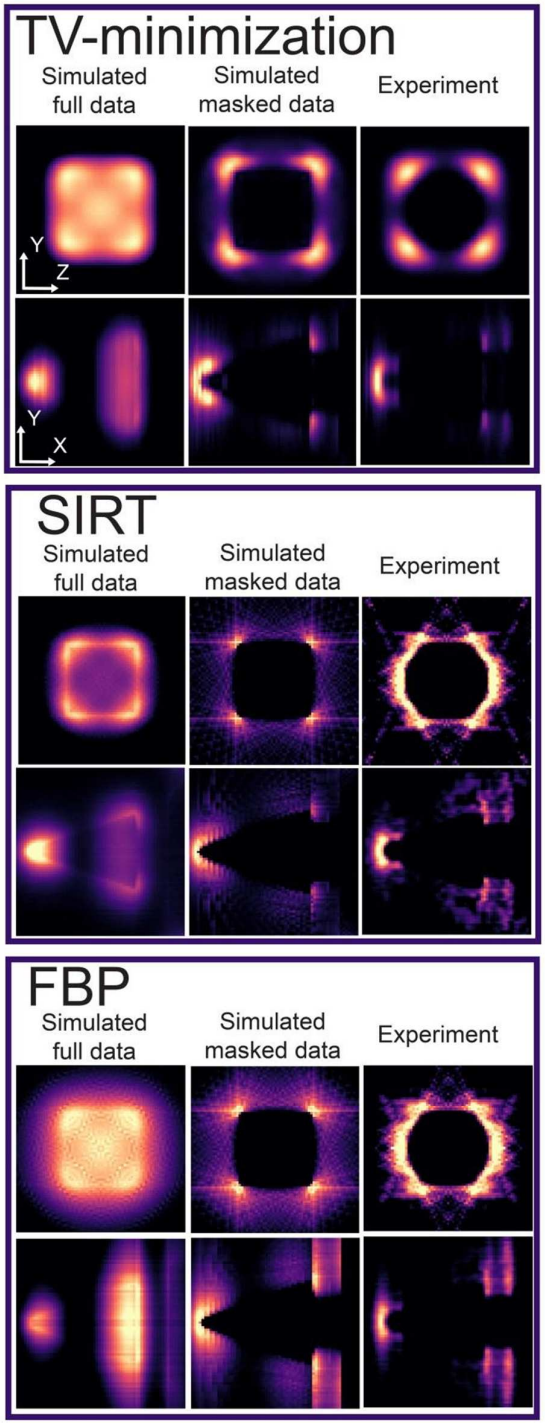

Fig. S5. Single slices from the STEM-EELS 3D tomography reconstruction for the first LSRP mode using TV-minimization, SIRT and FBP algorithms. The top YZ slices are from the base of the pyramid perpendicular to the axis of the tip (perpendicular to the tomography axis). The bottom YX slice for each reconstruction algorithm are taken from the center of the pyramid along its axis. The Z axis coincides with the electron trajectory.

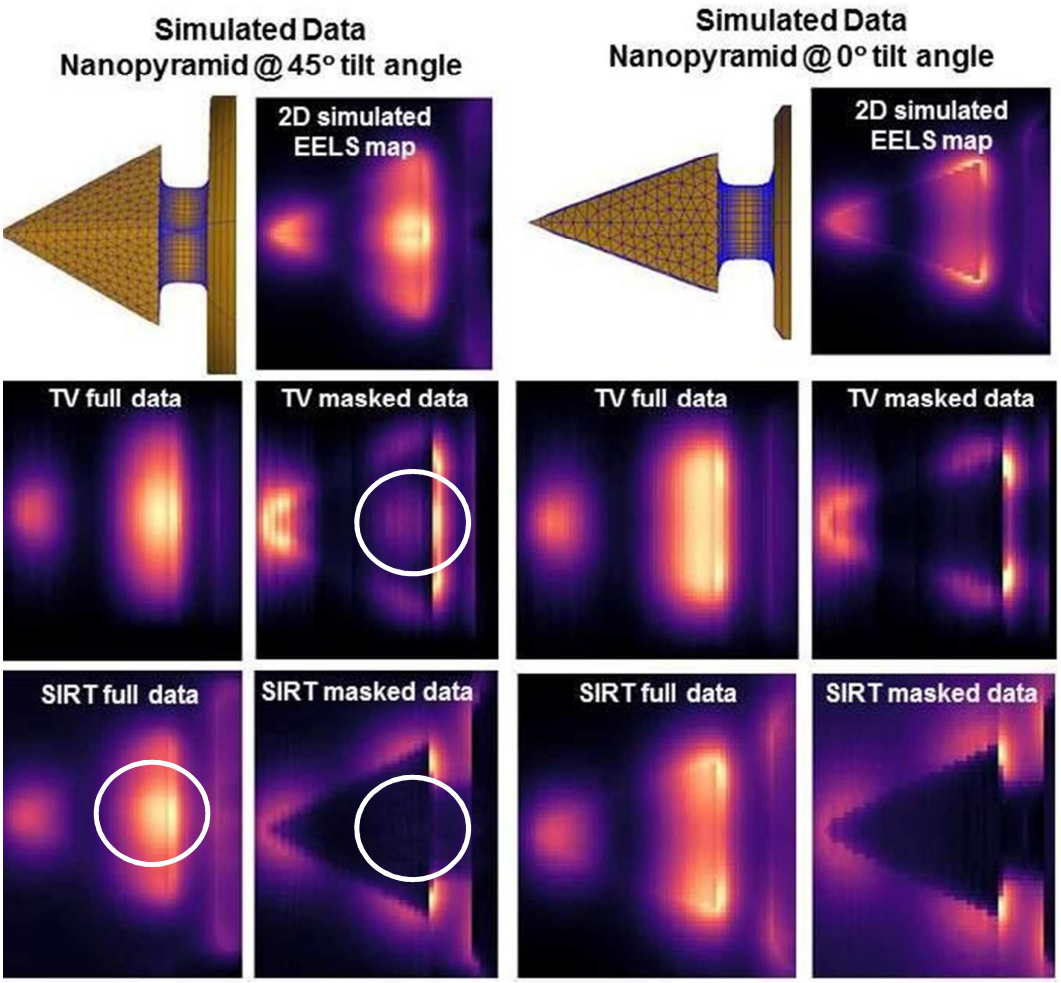

Fig. S6 Here we compare the projections of the reconstructed simulated full and masked data sets to the simulated 2D EELS maps. On top part of the figure we show the schemes of surface mesh used in MNPBEM simulation and their respective 2D EELS maps, one perpendicular to the pyramid edge (45° tilt angle) and another perpendicular to the pyramid face (0° tilt angle). The projections were calculated using the Matlab function radon. We can notice the better performance of TV-minimization when using masked data by analyzing the circled regions in the figure. Part of the information is recovered as the circled hotspot is seen in the projection of the TV-minimization reconstructions of masked data. This hotspot is not present in the projection of the SIRT reconstructions of the masked data. Therefore the projections of the TV-minimization reconstructions of masked data better matches the projections of the SIRT reconstructions of full data.

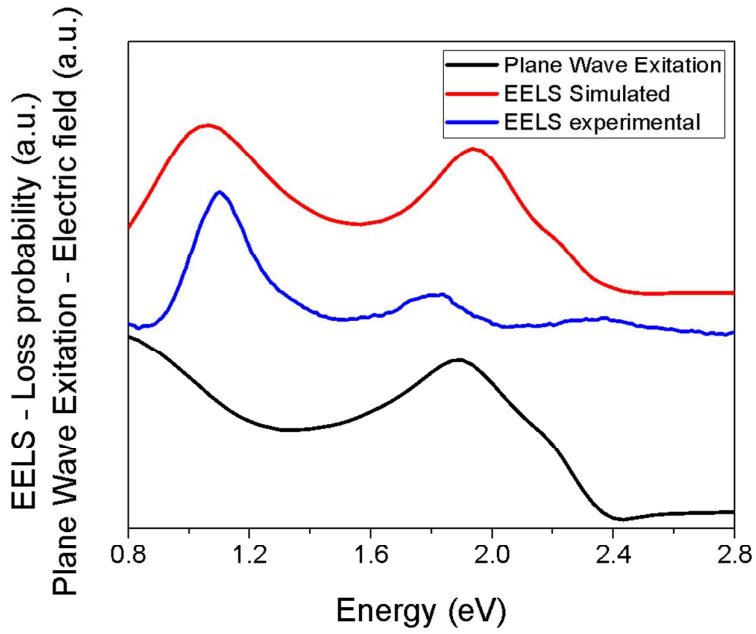

Fig S7. Electron loss probability simulated (EELS-MNPBEM) and experimental compared to simulated (optical excitation MNPBEM) electric field enhancement through plane wave excitation in the 0.8 up to 2.8 eV energy range.

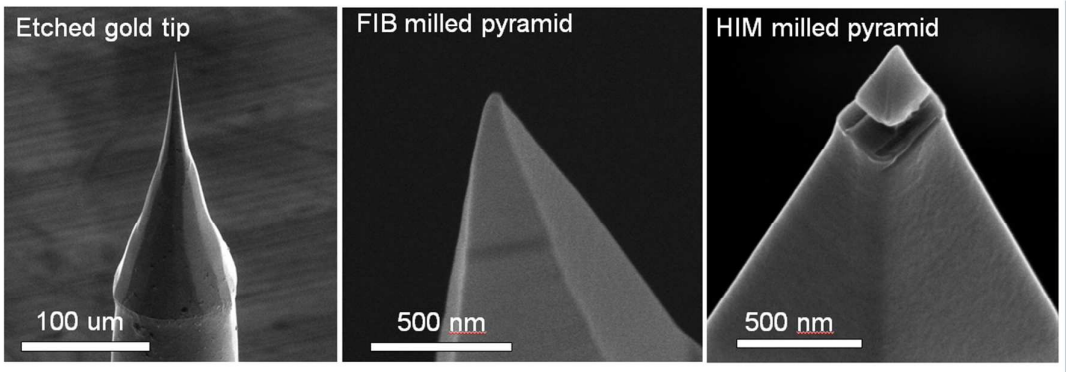

Fig S8. Images of the gold tip after each step fabrication: Electrochemical etching, FIB coarse fabrication and HIM fine fabrication.

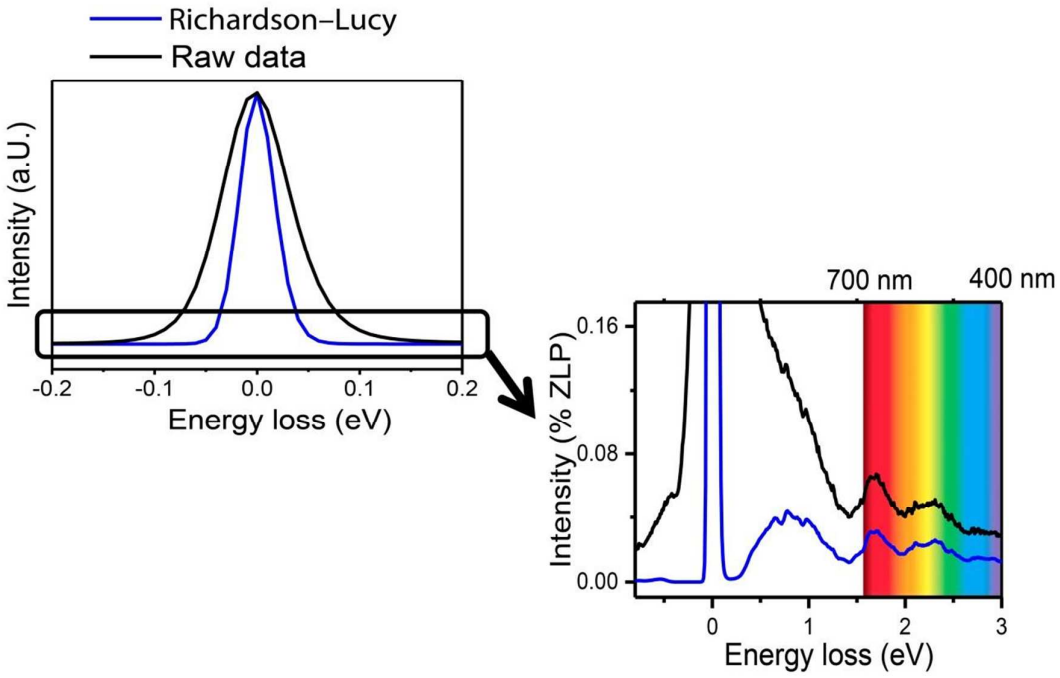

Fig. S9 – Richardson-Lucy deconvolution applied to a single spectrum used in this work.

Table S1 – Results from the MNPBEM numerical simulations summarizing the nanopyramid parameter in order to have LSPR modes with energy in the range of the visible electromagnetic spectrum. Complementary to Fig. 2 of the main text.

LSPR modes in the visible optical range			
Size (nm) \opening angle(°)	**θ<30**	**30< θ<40**	**40< θ<60**
L<250	X	1st LSPR	1st LSPR
250<L<300	X	1st and 2nd LSPR	1st and 2nd LSPR
300<L<450	X	2nd LSPR	2nd LSPR
450<L<600	X	3rd LSPR	2nd and 3rd LSPR
600<L<800	X	3rd LSPR	3rd LSPR